

Changes in the Asian monsoon climate during 1700–1850 induced by preindustrial cultivation

Kumiko Takata^{a,1}, Kazuyuki Saito^{a,b}, and Tetsuzo Yasunari^{a,c}

^aResearch Institute for Global Change, Japan Agency for Marine–Earth Science and Technology, 3173-25 Showa-machi, Kanazawa-ku, Yokohama, Kanagawa 236-0001, Japan; ^bInternational Arctic Research Center, University of Alaska Fairbanks, P.O. Box 757340, Fairbanks, AK 99775-7340; and ^cHydrospheric Atmospheric Research Center, Nagoya University, Furo-cho, Chikusa-ku, Nagoya, Aichi 464-8601, Japan

Edited by Ray S. Bradley, University of Massachusetts, Amherst, MA, and accepted by the Editorial Board April 15, 2009 (received for review July 31, 2008)

Preindustrial changes in the Asian summer monsoon climate from the 1700s to the 1850s were estimated with an atmospheric general circulation model (AGCM) using historical global land cover/use change data reconstructed for the last 300 years. Extended cultivation resulted in a decrease in monsoon rainfall over the Indian subcontinent and southeastern China and an associated weakening of the Asian summer monsoon circulation. The precipitation decrease in India was marked and was consistent with the observational changes derived from examining the Himalayan ice cores for the concurrent period. Between the 1700s and the 1850s, the anthropogenic increases in greenhouse gases and aerosols were still minor; also, no long-term trends in natural climate variations, such as those caused by the ocean, solar activity, or volcanoes, were reported. Thus, we propose that the land cover/use change was the major source of disturbances to the climate during that period. This report will set forward quantitative examination of the actual impacts of land cover/use changes on Asian monsoons, relative to the impact of greenhouse gases and aerosols, viewed in the context of global warming on the interannual, decadal, and centennial time scales.

atmospheric water balance | climate change |
historical land-cover change | monsoon rainfall

In general, a monsoon is generated from a thermal contrast between land and ocean. Thus, the land's surface condition is an important factor in determining its climate. Monsoon Asia, where >50% of the world population is concentrated, has experienced large land cover/use changes due to agricultural development, particularly during the 18th and 19th centuries. In India and China between 1700 and 1850, extension of cultivation and habitation activities decreased the percentage of forested area from 40–50% to 5–10% of the entire territories between 1700 and 1850 (1).

Changing the land cover/use from forest to croplands can affect the global and regional climate through changes in the energy and water balance at the earth's surface (2, 3). Among the various effects of vegetation change, 2 factors have been shown to have a major influence on the energy and water balance: (i) an increase in surface albedo leading to a reduction in solar energy absorption at the surface and (ii) a decrease in surface roughness, resulting in low-level wind speed intensification. As a consequence, the partitioning of turbulent heat fluxes into its sensible and latent heat fluxes would subsequently affect the planetary boundary layer and deep cumulus convection and, hence, the large-scale atmospheric phenomena (3). Previous modeling studies that investigated the impact of those effects used either a model of intermediate complexity with historical land cover changes (4, 5) or a general circulation model with a simplified setup in which the indigenous forests were totally and uniformly replaced by cultivated land. These latter studies have shown how different vegetation distributions affect the global surface energy–water balance (6, 7) or the atmospheric circulation (8, 9). In the Asian tropical region, the effect of reduced roughness on the summer climate was stronger than the effect of

increased albedo on a simplified setup (10). Yet, a detailed examination or discussion of these distinct effects due to the historical changes has been insufficient.

Here, we examine the actual impacts of land cover/use changes using a global historical vegetation map reconstructed for the last 300 years (1, 11). In the first half of the period, from 1700 to 1850, intensive cultivation activities continually occurred over the Indian subcontinent and over eastern China in Asia (shaded areas in Fig. 1). Croplands in India have continued to increase since the 17th century (1) when the British East India Company embarked on the colonial management in the Mughal Empire. Croplands expanded explosively in China in the 1700s (1) in response to the introduction of new crops (e.g., corn, sweet potato, peanut) and to the rapid increase in population under the favorable economic policies of the Qing Dynasty.

We considered that the difference between the climatic realizations of the 2 periods, in the 1700s and in the 1850s, might represent the long-term changes that occurred in those 150 years, and we examined the impacts of the reconstructed historical land cover/use changes between those 2 periods. Consequently, we conducted 2 time-slice numerical experiments for the periods represented by 1700 and 1850, using the historical vegetation maps of 1700 and 1850 (1,11) [see [supporting information \(SI\) Fig. S1](#)] as the lower boundary conditions for an atmospheric general circulation model (AGCM) (12), considering the changes in physical and physiological parameters of vegetation. Both equilibrium experiments were repeatedly forced by identical climatological annual cycles of the present-day monthly distributions of sea surface temperature (SST) and sea ice. The averaged states of summer (June, July, and August) were computed for the equilibrated results. These were compared for examining the impact of the land cover/use changes on the Asian summer monsoons between the 2 periods.

Results

Changes in Wind Field and Surface Energy–Water Balance Between 1700 and 1850. In the western Indian subcontinent and in southeastern China, the summer monsoonal wind blows from the ocean to the land in the lower troposphere (streamlines in Fig. 1). Because winds usually decelerate over land because of the large surface roughness, atmospheric moisture convergence and, hence, precipitation are large in those regions. Most of the agricultural cultivation during 1700–1850 occurred on forest (see [SI Text](#) and [Fig. S1](#)), causing the surface roughness to decrease because of the reductions in vegetation height and leaf amount [specified as leaf area index (LAI)]. As a result, the surface wind speed increased (colors in Fig. 2A). This effect reached the lower

Author contributions: T.Y. designed research; K.T. and K.S. performed research; T.Y. provided validation data; K.T. and K.S. analyzed data; and K.T. and K.S. wrote the paper.

The authors declare no conflict of interest.

This article is a PNAS Direct Submission. R.S.B. is a guest editor invited by the Editorial Board.

¹To whom correspondence should be addressed. E-mail: takata@jamstec.go.jp.

This article contains supporting information online at www.pnas.org/cgi/content/full/0807346106/DCSupplemental.

Table 1. Atmospheric moisture budget of the June–August mean in millimeters-month⁻¹

Year	Western Indian subcontinent		Southeastern China		Mideastern China	
	1700	1850	1700	1850	1700	1850
Moisture convergence	146.1	77.4	139.8	108.3	22.4	33.2
Evapotranspiration	135.8	126.6	133.2	130.7	128.3	123.1
Precipitation	281.9	204.0	273.0	239.0	150.7	156.3

Moisture convergence, evapotranspiration, and precipitation in the western Indian subcontinent (72–80°E, 17–25°N), southeastern China (105–115°E, 20–27°N) and the middle of eastern China (105–120°E, 27–37°N).

peratures, solar activity, and volcanic eruptions could have caused climate change, but there are no reports of remarkable trends or substantial changes in these factors that are comparable to the changes in land cover/use. The solar constant, according to the reconstructed variation for 1713–1996 (16), had a clear decadal solar cycle, but there was no apparent trend from 1713 to 1850. A few major volcano eruptions occurred during that period (e.g., in 1783, 1809, 1815, and 1883) (17, 18). However, the effect of an individual eruption could have lasted no more than a decade, so no significant impact on the 1700s or 1850s climate was expected. These findings suggest that the simulated differences in the Asian monsoon climate between 1700 and 1850 reflect the results of land cover/use changes during that period.

We compared our results to the available estimates of preindustrial climate derived from proxy data and/or historical records. The monsoonal precipitation in the western Indian subcontinent was negatively correlated to the annual snow accumulation at Dasuopu in the central Himalayas, according to a glacier ice-core analysis for the past 300 years (19). This analysis revealed that the monsoon precipitation in the region decreased by $\approx 20\%$ (i.e., ≈ 200 mm) from the 1700s to the 1850s (see Fig. S5). Another glacier ice-core analysis at Qomolangma (Mount Everest, Himaraya), spanning 1534–2001, revealed a decrease in annual precipitation from the 1700s to the 1850s that was significantly correlated with the all-India precipitation (20). These results are qualitatively and quantitatively consistent with our simulated result. This high level of agreement might be related to the “hot spots,” one of which is located in India, where the impact of the lower boundary conditions (e.g., soil moisture) on precipitation has been shown to be very high (21).

Using historical vegetation maps, we found that the actual land cover/use change had a significant impact on the energy and water budget and on the atmospheric circulation in summer

Asian monsoon regions. The simulated changes in precipitation in the Indian subcontinent agreed well with the reconstructed climate estimates for 1700–1850, when the only significant agent for the long-term trend that we identified was land cover/use change. In contemporary times, changes in land cover/land use need to combine with increases in greenhouse gases and aerosols to impact the Asian monsoon climate.

Methods

Model Description. We used an AGCM that was the atmospheric component of a global climate model, Model for Interdisciplinary Research on Climate (MIROC) version 3.2 (12), with a land surface scheme, Minimal Advanced Treatments of Surface Interaction and Runoff (MATSIRO) (22). Land cover/use was categorized into 11 vegetation types (see Fig. S1). The vegetation parameters (canopy top/bottom height, leaf reflectance/transmissivity, leaf turbulent exchange coefficients, and photosynthetic parameters) were determined for each vegetation type and were prescribed at each grid point according to the assigned vegetation type. We specified the monthly LAI at each grid point; these values were derived from a satellite observation independent of the vegetation distribution. Surface albedo and surface roughness were estimated from the above parameters, by using a single-layer canopy scheme on the basis of a multilayer canopy model (23, 24). Stomatal resistance for transpiration was estimated with a simple photosynthetic scheme (25). Energy and water balances at leaf and ground surfaces were determined by all of the above factors and processes, including snow, runoff, ground thermal and hydrological processes, and canopy water balance.

The AGCM used a 2-stream k -distribution method for radiation, a prognostic Arakawa–Schubert cumulus scheme, a prognostic cloud water scheme for large-scale condensation, a turbulence closure scheme with cloud effects, and an orographic gravity wave drag scheme. The primitive equations on a sphere using a spectral transform method were used for the dynamical part, for prognosticating the wind velocity, temperature, surface pressure, and mixing ratio of water vapor and cloud liquid water. See ref. 12 for the details.

Experimental Settings. The numerical experiments were conducted by using the AGCM with 20 vertical levels and a horizontal resolution of spectral triangular 42 (T42, i.e., $\approx 2.8^\circ$, ≈ 300 km). The historical vegetation distribution was prescribed for each 50-year integration, represented by the years 1700 and 1850 (see Fig. S1). The vegetation map (11) was produced by superimposing the historical croplands ratio (1) onto the present day (i.e., in 1992) land cover map (U.S. Geological Survey Global Land Cover Characterization, Version 1.2, 2003, <http://edc2.usgs.gov/glcc/glcc.php>). For any grid point where the cropland ratio was smaller than the threshold value (11), the potential vegetation (1) was assigned.

A climatological annual cycle of LAI distribution was produced for the historical vegetation map (11), by superimposing the monthly LAI for potential vegetation onto the present-day monthly mean LAI map averaged from 1983 to 1995 in International Satellite Land Surface Climatology Project Initiative 2 (ISLSCP-II) dataset (26). The monthly LAI for potential vegetation was estimated by averaging the present-day LAI for the same vegetation type at the same 5° latitude band for each month (11).

Similar to the LAI, climatological annual cycles of SST and sea ice distributions, derived from the observed monthly mean averaged from 1981 to 2000 (27) was prescribed throughout the integrations in this study.

Identical initial conditions for the atmosphere and land were used for both integrations; these resulted from an equilibrated integration with the present-day land use condition. Because the vegetation distribution and the annual cycles of LAI, SST, and sea ice are all fixed, the interannual variability, after reaching an equilibrated state, is solely induced by the internal variability of the atmosphere–land system. Thus, the differences between the aver-

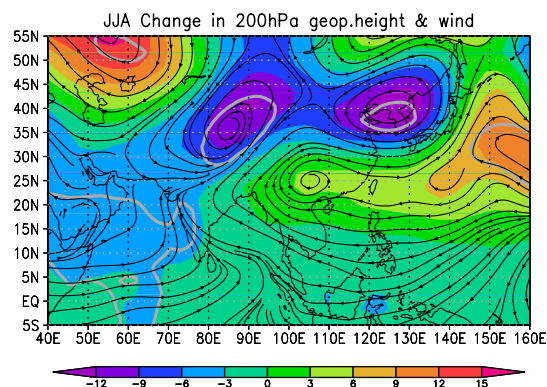


Fig. 3. June–August mean changes in the 200-hPa wind field (streamlines) and geopotential height (colors, in meters) between 1700 and 1850. Thick gray lines represent those in which the differences are statistically significant at the 95% confidence level.

ages of the 2 experiments, calculated from the equilibrated 40 years of the 50-year integrations, showed that the signal resulted from the land cover/use change and did not reflect the initial conditions. The statistical significance of any difference between the 2 experiments was examined by *t* test, with the interannual variability as the measure of the noise. The values in the summer season (July to August) were used in the analysis, which is when the Asian monsoon activity is at its highest.

- Ramankutty N, Foley JA (1999) Estimating historical changes in global land cover: Croplands from 1700 to 1992. *Global Biogeochem Cycles* 13:997–1027.
- Pielke RA, Sr, et al. (2002) The influence of land-use change and landscape dynamics on the climate system: Relevance to climatic-change policy beyond the radiative effect of greenhouse gases. *Phil Trans R Soc London Ser A* 360:1705–1719.
- Kabat P, et al., eds (2004) Vegetation, water, humans and the climate: A new perspective on an interactive system. *Global Change—The IGBP Series* (Springer, Berlin).
- Brovkin V, et al. (2004) Role of land cover changes for atmospheric CO₂ increase and climate change during the last 150 years. *Glob Change Biol* 10:1253–1266.
- Brovkin V, et al. (2006) Biogeophysical effects of historical land cover changes simulated by six Earth system models of intermediate complexity. *Clim Dyn* 26:587–600.
- Bounoua L, Defries R, Collatz GJ, Sellers P, Khan H (2002) Effects of land cover conversion on surface climate. *Clim Change* 52:29–64.
- Feddema J, et al. (2005) A comparison of a GCM response to historical anthropogenic land cover change and model sensitivity to uncertainty in present-day land cover representations. *Clim Dyn* 25:581–609.
- Chase TN, Pielke RA, Sr, Kittel TGF, Nemani RR, Running SW (2000) Simulated impacts of historical land cover changes on global climate in northern winter. *Clim Dyn* 16:93–105.
- Zao M, Pitman AJ, Chase T (2001) The impact of land cover change on the atmospheric circulation. *Clim Dyn* 17:467–477.
- Mabuchi K, Sato Y, Kida H (2005) Climatic impact of vegetation change in the Asian tropical region. Part I: Case of the Northern hemisphere summer. *J Clim* 18:410–428.
- Hirabayashi Y, Kanae S, Struthers I, Oki T (4 October 2005) A 100-year (1901–2000) global retrospective estimation of the terrestrial water cycle. *J Geophys Res*, 10.1029/2004JD005492.
- K-1 Model Developers (2004) K-1 coupled model (MIROC) description. *K-1 Tech Rep No. 1*, eds Hasumi H, Emori S (Center for Climate System Research, Univ of Tokyo, Kashiwa, Chiba, Japan), pp1–34.
- Fu K (2003) Potential impacts of human-induced land cover change on East Asia monsoon. *Glob Planet Change* 37:219–229.
- Abe M, Yasunari T, Kitoh A (2004) Effects of large-scale orography on the coupled atmosphere–ocean system in the Tropical Indian and Pacific Oceans in boreal summer. *J Meteorol Soc Jpn* 82:745–759.
- Forster P, et al. (2007) Changes in atmospheric constituents and in radiative forcing. *Climate Change 2007: The Physical Science Basis. Contribution of Working Group I to the Fourth Assessment Report of the Intergovernmental Panel on Climate Change*, eds Solomon S, et al. (Cambridge Univ Press, Cambridge, UK), pp129–234.
- Wang Y-M, Lean JL, Sheeley NR, Jr (2005) Modeling the sun's magnetic field and irradiance since 1713. *Astrophys J* 625:522–538.
- Robock A (March 16, 2005) Cooling following large volcanic eruptions corrected for the effect of diffuse radiation on tree rings. *Geophys Res Lett*, 10.1029/2004GL022116.
- Gao C, Oman L, Robock A, Stenchikov GL (May 8, 2007) Atmospheric volcanic loading derived from bipolar ice cores: Accounting for the spatial distribution of volcanic deposition. *J Geophys Res*, 10.1029/2006JD007461.
- Duan K, Yao T, Thompson LG (August 25, 2004) Low-frequency of southern Asian monsoon variability using a 295-year record from the Dasuopu ice core in the central Himalayas. *Geophys Res Lett*, 10.1029/2004GL020015.
- Kaspari S, et al. (2008) Snow accumulation rate on Qomolangma (Mount Everest), Himalaya: Synchronicity with sites across the Tibetan plateau on 50–100 timescales. *J Glaciol* 54:343–352.
- The GLACE team: Koster RD, et al. (2004) Regions of strong coupling between soil moisture and precipitation. *Science* 305:1138–1140.
- Takata K, Emori S, Watanabe T (2003) Development of the minimal advanced treatments of surface interaction and runoff. *Glob Planet Change* 38:209–222.
- Watanabe T, Ohtani Y (1995) A simple model of shortwave-radiation transport within canopy. *J Agric Meteorol* 51:57–60 (in Japanese).
- Watanabe T (1994) Bulk parameterization of a vegetated surface and its application to a simulation of nocturnal drainage flow. *Boundary-Layer Meteorol* 70:13–35.
- Sellers PJ, et al. (1996) A revised land surface parameterization (SiB2) for atmospheric GCMs. Part I: Model formulation. *J Clim* 9:676–705.
- Hall FG, et al. (2004) *ISLSCP Initiative II* (CD-ROM) (Natl Aeronautics and Space Administration, Greenbelt, MD).
- Taylor KE, Williamson D, Zwiers F (2000) The sea surface temperature and sea-ice concentration boundary conditions for AMIP II simulations. *PCMDI Report No. 60* (Program for Climate Model Diagnosis and Intercomparison, Lawrence Livermore Natl Lab, Livermore, CA), pp1–25.

ACKNOWLEDGMENTS. We thank Dr. Y. Hirabayashi (Jichi Medical University, Tochigi, Japan) for providing the historical vegetation maps, and Dr. Y. Kosaka and Mr. R. Yamashima for data analysis and visualization assistance. The authors are also grateful to the editor and the 2 anonymous reviewers for providing valuable comments in the revision of the article. This work was supported by the Global Environment Research Fund of the Ministry of the Environment, Japan (B-061). All numerical integrations were run on the NEC SX-8 supercomputer at the Japan Agency for Marine–Earth Science and Technology.

Supporting Information

Takata et al. 10.1073/pnas.0807346106

SI Text

Global maps of vegetation in 1700 and 1850 are shown in Fig. S1. The red areas indicate cultivated areas. Most of the cultivated land was originally forest, except for a few grid points (e.g., on the western edges of the cultivated area in eastern China). These areas had originally been grassland, and because vegetation height and LAI are similar for grasslands and croplands, the surface wind speed did not change at those points. The surface albedo was slightly decreased by <0.01 due to the larger LAI for croplands than for grasslands. However, the albedo decrease had no discernible effects because its area and magnitude were small. Large area was also cultivated intensively in Western Europe during 1700–1850. This land use/cover change may have an impact in the winter, but is generally insignificant in the summer.

We display the increase in surface wind speed that reached the lower troposphere by the longitude–height cross-sections of changes in the horizontal winds, in addition to the changes in 850-hPa wind vectors (Fig. 2A). The cross-section at 20°N shows that the westerly wind increased from 75°E to 85°E, which corresponds to the western Indian subcontinent (the IND region; Fig. S2a, shown by rightward vectors). The cross-section at 30°N shows that the southerly wind increased from 100°E to 120°E; this corresponds to southeastern China (SCH region; Fig. S2b, shown by upward vectors).

The effects of the reduction in clouds in the IND and SCH regions are clearly indicated by the increase in downward short-wave radiation (Fig. S3a). This corresponds with the regions where there was an increase in the net short-wave radiation absorbed at the surface (contours in Fig. 2C). Therefore, the increase in net short-wave radiation was induced by the increase in downward short-wave radiation, and hence the reduction in clouds, that is associated with a decrease in precipitation. In those regions, the surface soil moisture decreased, latent heat flux decreased, sensible heat flux increased, and air temperature at 2-m height increased (Fig. S3 b–e).

The effects of the increase in surface albedo appeared as a decrease in net short-wave radiation in ECH (Fig. 2C), occurring without a considerable decrease in downward short-wave radiation (Fig. S3a). In addition, outgoing long-wave radiation increased (Fig. S3f), as a result of the increase in the upward terrestrial radiation due to the surface temperature increase (Fig. S3g) and as a result of the decrease in downward long-wave radiation due to the moisture decrease near the surface (Fig. S3h). Summing those effects shows that the net radiation absorbed at the surface was decreased. A reduction in net radiation could result in a surface temperature decrease, but this effect appeared only at $\approx 30^\circ\text{N}$, 110–120°E, and was ≈ 0.5 –1 °C (Fig. S3e). At this location, surface soil moisture was not decreased (Fig. S3b).

JJA Changes in Sea level pressure

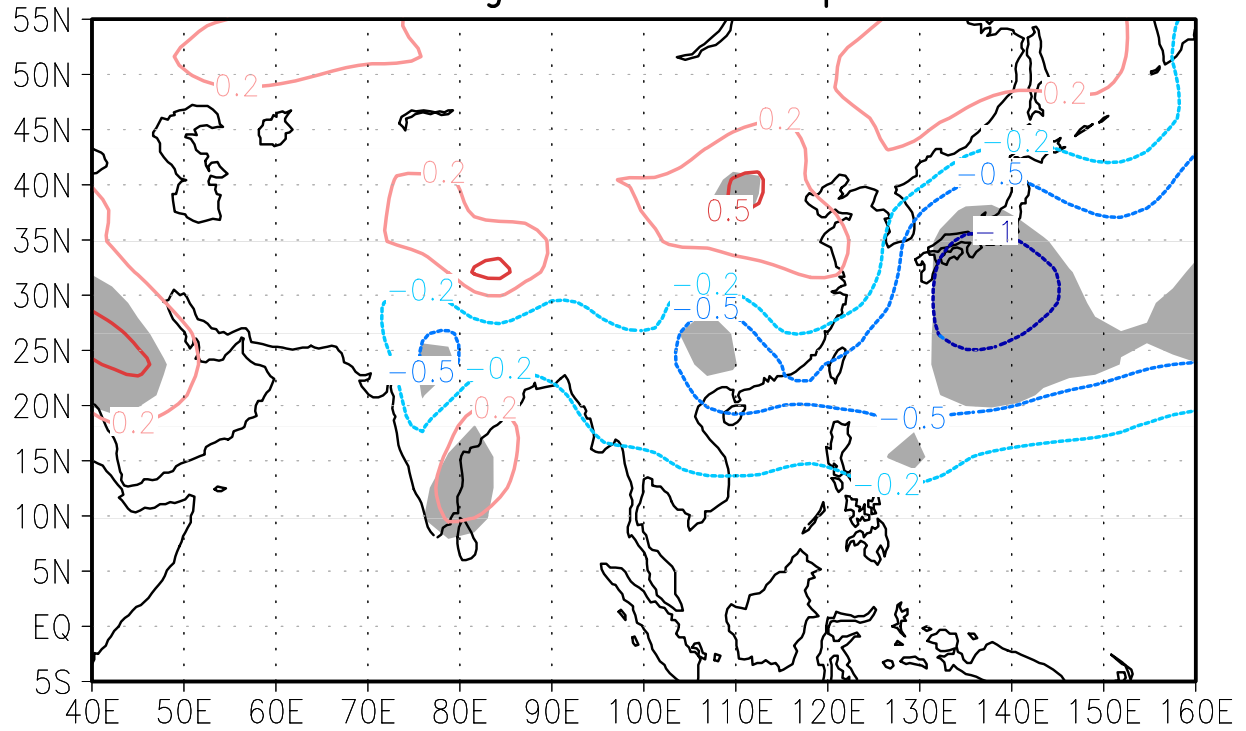


Fig. S4. June–August mean changes in sea level pressure (hPa) between 1700 and 1850. Shaded regions represent those in which the differences are statistically significant at the 95% confidence level.

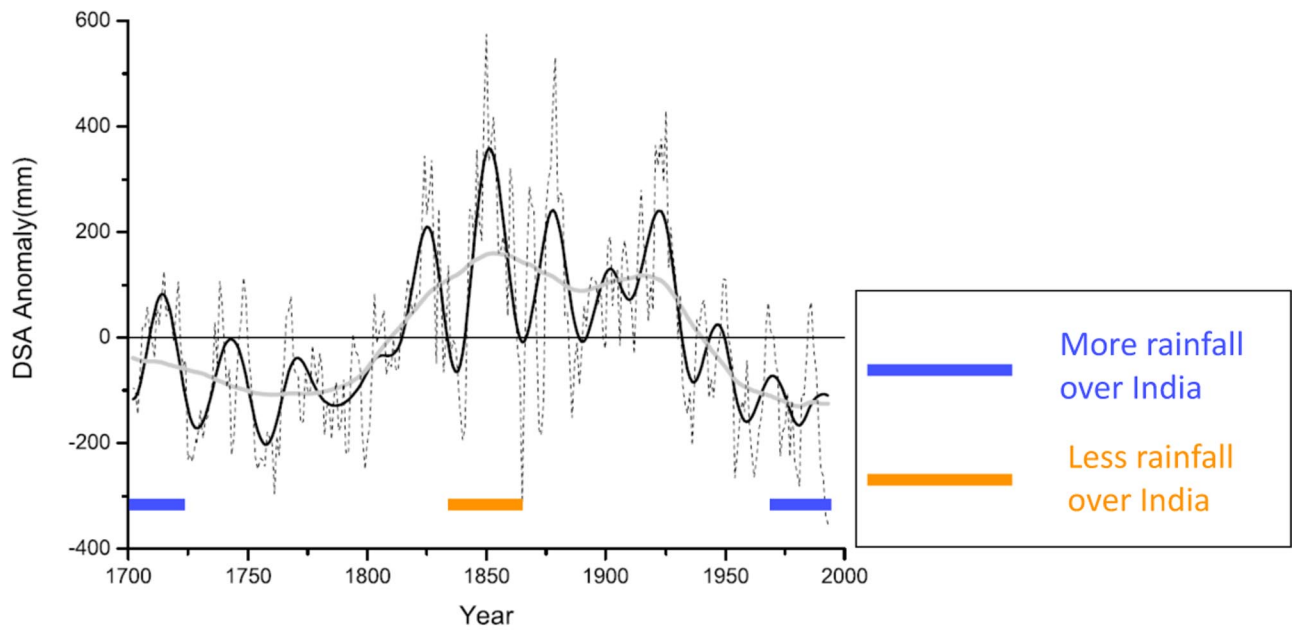


Fig. S5. Dasuopu snow accumulation (DSA) in Tibet–Himalaya and monsoon rainfall trends in Peninsula India (MRI). Three-year running mean of the DSA is shown by the dotted line, the reconstructed secular trend by the gray line, and the 26-year oscillation + trend by the solid line. MRI is negatively correlated with DSA (horizontal bars in lower part of the image) at a correlation coefficient of approximately -0.5 . After figure 4 of Duan K, Yao T, Thompson LG (August 25, 2004) Low-frequency of southern Asian monsoon variability using a 295-year record from the Dasuopu ice core in the central Himalayas. *Geophys Res Lett*, 10.1029/2004GL020015, modified by permission of the American Geophysical Union.